Available online at www.sciencedirect.com
SCIENCE DIRECT
Cement and Concrete Research 36 (2006) 1240–1251
Cement and Concrete Research

Microstructural and chemical effects of wet/dry cycling on pulp fiber–cement composites

B.J. Mohr [a,*], J.J. Biernacki [b], K.E. Kurtis [c]

[a] Department of Civil and Environmental Engineering, Tennessee Technological University, 1020 Stadium Drive, Box 5015, Cookeville, TN 38505-0001, USA
[b] Department of Chemical Engineering, Tennessee Technological University, 1020 Stadium Drive, Box 5013, Cookeville, TN 38505-0001, USA
[c] School of Civil and Environmental Engineering, Georgia Institute of Technology, 790 Atlantic Drive, Atlanta, GA 30332-0355, USA

Received 11 October 2005; accepted 23 March 2006

Abstract

The microstructural and chemical mechanisms responsible for pulp fiber–cement composite degradation during wet/dry cycling are being investigated through environmental scanning electron microscopy (ESEM), energy dispersive spectroscopy (EDS), and mechanical testing. Based on these results, a three-part progressive degradation mechanism for cast-in-place kraft pulp fiber–cement composites is proposed, which involves: (1) initial fiber–cement or fiber interlayer debonding, (2) reprecipitation of needle-like or sheath-like ettringite within the void space at the former fiber–cement interface or between the S1 and S2 fiber layers, and (3) fiber mineralization due to reprecipitation of calcium hydroxide filling the spaces within the fiber cell wall structure. This investigation also revealed that kraft pulp fibers exhibit poor resistance to degradation due to their inferior dimensional stability, as compared to thermomechanical pulp (TMP) fibers. TMP fibers contain significant amounts of lignin, which is alkali sensitive. Despite this, TMP fiber–cement composite exhibit improved resistance to degradation during wet/dry cycling. It is proposed that this improvement in durability may be attributed to the presence of lignin in the cell wall restricting fiber dimensional changes during wetting and drying, and hence, minimizing fiber–cement debonding. Additionally, it is proposed that lignin acts as physical barrier to calcium hydroxide formation within the fiber cell wall, minimizing fiber mineralization of TMP fibers.

Keywords: Degradation; Durability; EDX; Fiber reinforcement; SEM

1. Introduction

Wood pulp fiber–cement composites are primarily used in exterior applications where ensuring adequate performance with continued environmental exposure is essential. Most research regarding the durability of these materials has been concerned with assessing their mechanical properties after exposure to wet/dry cycling. Though the degradation of mechanical properties, particularly toughness, is fairly well-established [1–10], only limited research has been published that addresses the chemical and microstructural manifestations of composite degradation. For example, Bentur and Akers [11] found that pulp fibers become embrittled due to the formation of hydration products within the fiber lumen. Examining sisal fibers in cement-based composites, Tolêdo Filho et al. [12] and Savastano and Agopyan [13] have also confirmed the transport of cement hydration products, primarily CH (calcium hydroxide), within the fiber lumen, as well as around the fibers due to wet/dry cycling.

However, these observed microstructural changes are the end result of cycling; the mechanisms of degradation with continued wet/dry cycling have not been comprehensively examined in the published literature. Previous mechanical testing [7,8] has shown that composite mechanical property degradation does not occur linearly with increasing numbers of cycles. That is, the majority of losses in strength and toughness occurred with the first five wet/dry cycles. Thus, it seems reasonable to assume that there may be more than one microstructural mechanism contributing to composite degradation.

Based upon mechanical test data and some limited microscopy, Mohr et al. [7] proposed a three-part progressive degradation model for cast-in-place kraft pulp fiber–cement

* Corresponding author. Tel.: +1 931 372 3546; fax: +1 931 372 6239.
E-mail address: bmohr@tntech.edu (B.J. Mohr).

0008-8846/$ - see front matter © 2006 Elsevier Ltd. All rights reserved.
doi:10.1016/j.cemconres.2006.03.020

Table 1
Oxide analysis (mass percent) and Bogue potential composition for ASTM Type I portland cement

Oxide	Type I portland cement
SiO_2	20.17
Al_2O_3	5.34
Fe_2O_3	3.85
CaO	63.93
MgO	0.91
Na_2O	0.05
K_2O	0.35
TiO_2	0.35
Mn_2O_3	0.08
P_2O_5	0.07
SrO	0.07
BaO	0.02
SO_3	4.00
Loss on ignition	0.80
Insoluble residue	0.05
C_3S	54.16
C_2S	16.97
C_3A	7.64
C_4AF	11.70

composites during wet/dry cycling, which consists of (1) initial fiber–cement or fiber interlayer debonding, (2) reprecipitation of secondary ettringite within the void space created by the previous step, and (3) fiber embrittlement due to fiber cell wall mineralization. According to this conceptual model, prior to wet/dry cycling and the reprecipitation of ettringite, pulp fibers are largely free to shrink and swell without impedance. Upon drying, diametrical fiber shrinkage may create a capillary expulsive pressure on the pore solution residing within the fiber lumen. Such a pressure would cause the pore solution to be primarily expelled through the fiber ends and pits along the fiber. During this drying, reprecipitation of hydration products can occur in the void space created by debonding. However, the reprecipitation of hydration products, such as ettringite, in this space can restrain fiber swelling upon rewetting. During subsequent drying, then, fiber shrinkage is also reduced. Thus, the driving force for pore solution expulsion is minimized. That is, the pore solution resides within the fiber for a longer period of time. Therefore, the pore solution will not only migrate from the fiber lumen to the matrix through the ends and fiber pits, but the solution can also diffuse from the lumen through the cell wall, resulting in a deposition of hydration products, likely CH, within the fiber cell wall. This deposition or reprecipitation decreases fiber ductility and leads to shorter fiber pull-out lengths in the composite. Fiber embrittlement due to mineralization appears to occur beyond approximately 10 wet/dry cycles as indicated by slight increases in composite strength [7]. However, despite the correlation between the mechanical behavior and the conceptual model described above, further experimental investigation is necessary for verification and, potentially, for refinement of the model.

Thus, the main objective of this research is to provide microstructural and chemical data, obtained through environmental scanning electron microscopy (ESEM), to assess the validity of the proposed mechanism of degradation in cast-in-place kraft pulp fiber–cement composites exposed to wet/dry cycling. It is anticipated that the development of a progressive degradation model through microstructural and chemical degradation observations can lead to means for prevention and mitigation of composite degradation pulp fiber–cement composites.

2. Experimental study

2.1. Sample preparation

Pulp fiber–cement composites prepared for this study contained 4% unbleached kraft pulp, bleached kraft pulp, or thermomechanical pulp (TMP) fibers by volume. ASTM Type I portland cement, with oxide analysis and Bogue potential composition shown in Table 1, was used at a water-to-cement ratio of 0.60. The composites were subjected to 0, 1, 2, 5, 10, 15, or 25 wet/dry cycles prior to mechanical flexure testing at 78 days. A wet/dry cycle was defined as 23 h and 30 min drying in an oven at 65±5 °C and 20±5% RH, air drying at 22±5 °C and 60±5% RH for 30 min, 23 h and 30 min soaking in water at 20±2 °C, and air drying at 22±5 °C and 60±5% RH for 30 min.

All samples were cured in limewater for at least 28 days. Those samples subjected to a lower number of cycles remained in the limewater for longer periods of time, such that all samples were tested at the same age, to ensure that the influence of continued cement hydration with time did not impact the results. For example, samples that were exposed to 5 wet/dry cycles were continuously cured in limewater for 68 days, cycled over a 10-day period, and tested at 78 days. Mechanical flexure results for the kraft pulp and TMP fiber–cement composites have been previously presented [7,8].

After mechanical testing, the specimens were soaked in ethanol for 24 h and oven-dried at 105 °C for 48 h to dehydrate the sample and minimize further cement hydration. Following dehydration, samples were stored in sealed containers to minimize carbonation.

Additionally, samples for SEM backscattered electron (BSE) imaging were cut to a thickness of 5 mm using an Allied High Tech 4 variable speed wafering saw with ethanol as the cutting lubricant. After cutting, samples were dried at 105 °C for 1 h. Epoxy impregnation was accomplished using a Buehler vacuum impregnation system and EPO-THIN epoxy. Potted samples

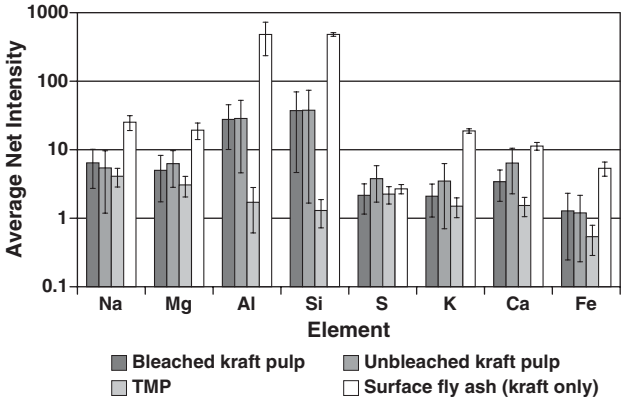

Fig. 1. ESEM EDS average elemental net intensity for fibers prior to mixing.

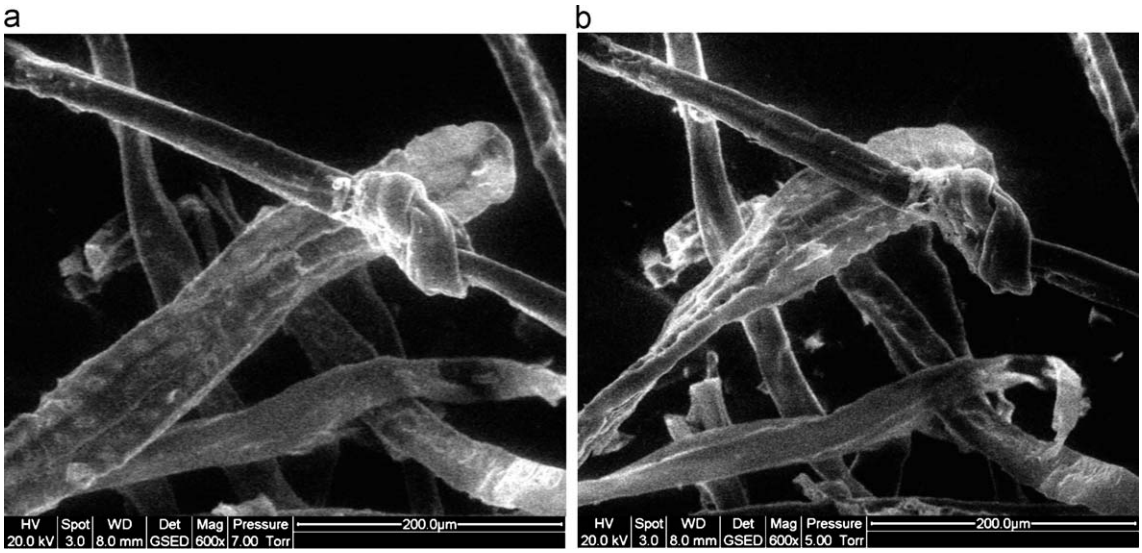

Fig. 2. TMP dimensional change capacity. (a) After 30 min at 100% RH. (b) After 5 min at 10% RH.

were manually polished using a Buehler Economet 4 variable speed grinder–polisher with sequential grit sizes of 240, 320, and 600 for 2 min each. Automatic final polishing was accomplished on a Buehler VECTOR grinder–polisher with 5 and 1 μm diamond aerosol sprays. Samples were cleaned with ethanol after each polishing step.

2.2. Environmental scanning electron microscopy

Microstructural observations were conducted on a FEI Quanta 200 environmental scanning electron microscope (ESEM) in a gaseous (water vapor) environment. In situ microscopic wet/dry cycling observations were made by mounting specimens on a thermocoupled stage. Specimen wetting and drying was accomplished by maintaining a constant stage temperature of 5 °C and changing the water vapor pressure in order to modify the local relative humidity. For observations of in situ saturation of fracture surfaces, samples were removed from the composite such that the sample thickness was several millimeters to ensure adequate water vapor condensation above the samples.

2.3. Energy dispersive spectroscopy

Initially, a Monte Carlo simulation was performed to determine an appropriate accelerating voltage (i.e., 10 kV) to ensure that the measurements were made on the fiber surface and within the fiber cell wall. Thus, the analysis excluded any mineral phases present in the fiber lumen. The maximum interaction depth was less than approximately 1.5 mm. As a result, the energy dispersive spectroscopy (EDS) results encompass only the hydration products apparent on the fiber surface and within the fiber cell wall.

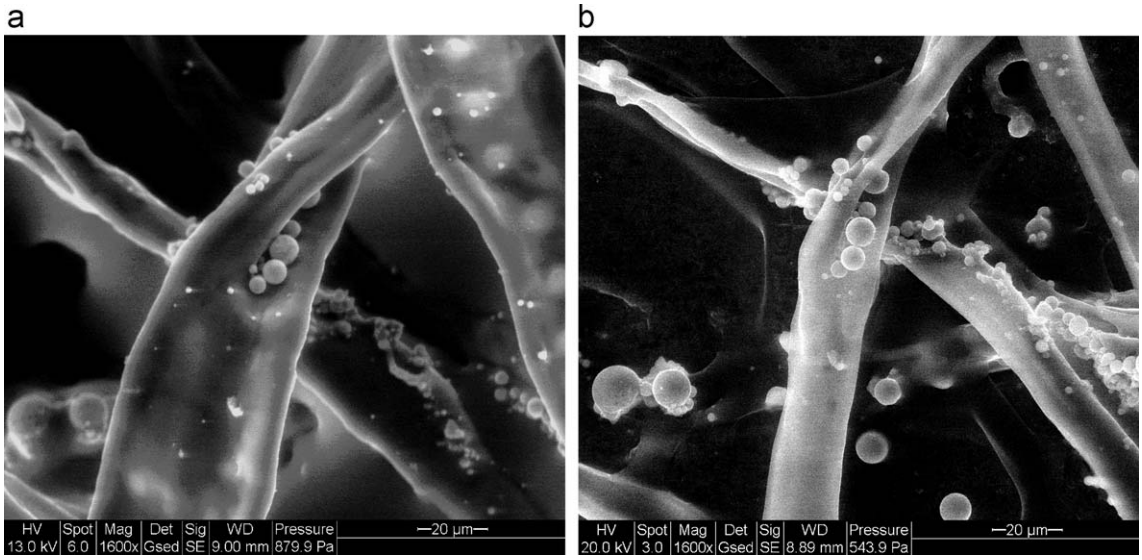

Fig. 3. Kraft pulp fiber dimensional change capacity. The spherical particles are fly ash, used to improve kraft pulp fiber dispersion. (a) After 30 min at 100% RH. (b) After 5 min at 10% RH.

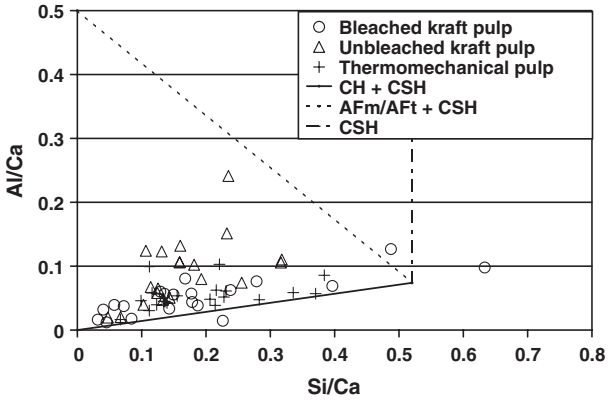

Fig. 4. Average Al/Ca versus Si/Ca molar ratios after 0 cycles.

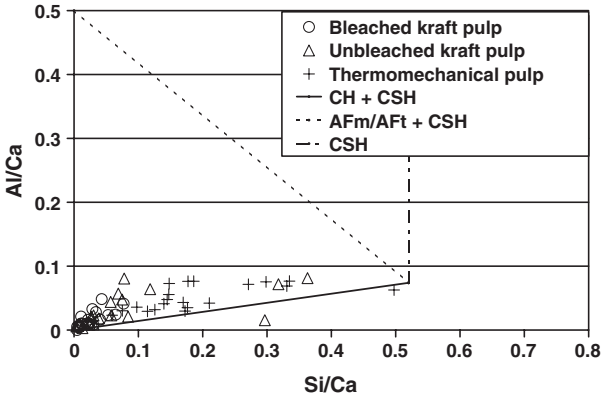

Fig. 6. Average Al/Ca versus Si/Ca molar ratios after 1 cycle.

Spectroscopy was accomplished using an EDAX SUTW detector. All EDS spectra were collected at an accelerating voltage of 10.0 kV and a water vapor pressure of 93.3 Pa (0.70 Torr). EDS measurements were standardized against a blast furnace slag with a previously known chemical composition, as in [14]. The standard was compared against a synthetic ettringite sample to verify the quantization. Certain conditions (e.g., spot size) varied to obtain adequate ESEM images or facilitate EDS spectra collection.

For the composite fracture surfaces, several EDS spot analyses were conducted on each observed fiber in secondary electron (SE) mode. One data point represents the average chemical composition of an observed fiber. Twenty fibers on each fracture surface were observed.

Additionally, to determine the approximate chemical composition of the matrix C–S–H, epoxy impregnated and polished composite samples were examined in backscattered electron (BSE) mode. Fifty data points were acquired for each sample examined.

3. Results and discussion

To assess the three-part progressive wet/dry cycling degradation mechanism proposed by Mohr et al. [7], kraft pulp and TMP fibers were examined via ESEM to quantify fiber dimensional changes during in situ saturation. Composite fracture surfaces were also examined to determine the fiber cell wall chemical composition prior to and after exposure to wet/dry cycling. As previously noted, the proposed progressive degradation mechanism consists of: (1) initial fiber–cement/fiber interlayer debonding, (2) reprecipitation of ettringite within the void space at the former fiber–cement interface or between the S1/S2 fiber layers, restricting subsequent fiber swelling, and (3) fiber embrittlement (i.e., fiber cell wall mineralization) caused by the diffusion of CH from the fiber lumen through the cell wall.

This model is intended for cast-in-place pulp fiber–cement composites. The use of other manufacturing methods may minimize or prevent the first two degradation steps. Due to the pressure induced during certain manufacturing techniques (e.g., Hatschek process), the fiber may be compressed and after setting, may not exhibit substantial dimensional changes upon wetting and drying. Thus, fiber–cement debonding and subsequent ettringite reprecipitation would be minimized. However, in these situations, composite degradation may proceed directly to the last step – calcium hydroxide reprecipitation within the fiber cell wall – hastening fiber mineralization. Composites manufactured via the Hatschek process also have the potential for lamina swelling and subsequent debonding of the lamina.

The following sections will begin by describing the dimensional stability and chemical composition of the pulp fibers (bleached kraft, unbleached kraft, and TMP) prior to mixing. The composition of the matrix C–S–H will then be investigated to

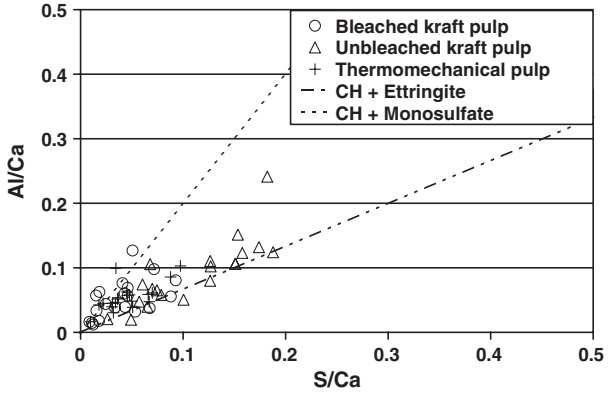

Fig. 5. Average Al/Ca versus S/Ca molar ratios after 0 cycles.

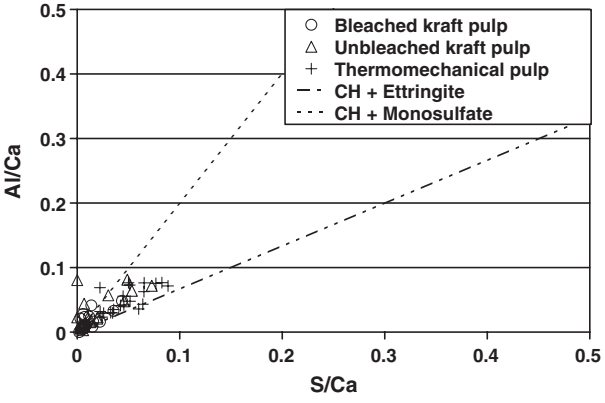

Fig. 7. Average Al/Ca versus S/Ca molar ratios after 1 cycle.

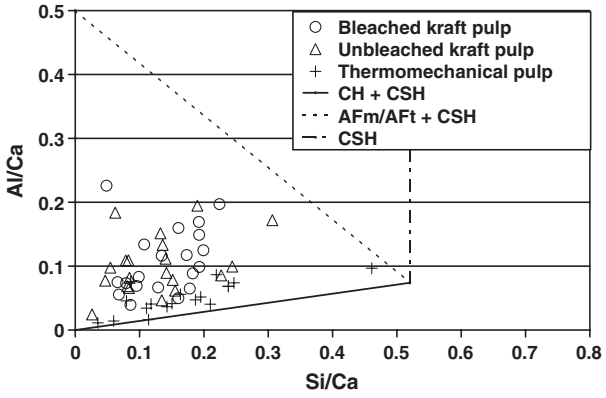

Fig. 8. Average Al/Ca versus Si/Ca molar ratios after 2 cycles.

determine if any changes in C–S–H composition occurred during wet/dry cycling. Results will also be presented regarding the original chemical composition of the pulp fiber surfaces and cell wall, prior to cycling. Subsequent sections will corroborate each step of aforementioned proposed degradation mechanism based on observed microstructural and chemical changes.

3.1. Pulp fiber characteristics

ESEM EDS observations were conducted on unbleached and bleached kraft pulp fibers as well as TMP fibers alone (i.e., in the absence of a cementitious matrix) to qualify fiber chemical composition. The fibers were also examined for dimensional changes during wetting and drying.

Results, shown in Fig. 1, indicate that the kraft fibers exhibited higher net intensities of Al and Si, than the TMP fibers. The kraft fibers were treated with a coupling agent and a supplementary cementitious material (SCM), using a process described in [15,16], to improve their dispersion. Therefore, the increased levels of alumina and silica on the kraft fiber surface can be attributed to the presence of the SCM on the fiber surface. The TMP fibers were not treated by this process, thus explaining the lower levels of inorganic elements on the fiber surface. In addition, examination of the kraft fibers did not yield any evidence of high alkali surface compositions (e.g., sodium) that may have been present due to the kraft pulping process.

Furthermore, dimensional changes during wetting and drying were observed for the kraft and TMP fibers. As seen in Fig. 2, the apparent dimensional changes in TMP fibers were much less than that of kraft fibers (Fig. 3). Average TMP fiber lateral swelling was approximately 10% compared to 135% for the kraft fibers. It should also be noted that TMP fiber swelling resulted in an apparent "straightening" of the fibers, whereas kraft fiber swelling was primarily observed as an increase in the lateral fiber dimension. These differences in dimensional stability are primarily due to the fiber lignin content [17]. Lignin stiffens the fiber cell wall by filling the spaces between the cellulose microfibrils improving dimensional stability, albeit at the sacrifice of fiber tensile strength on a unit weight basis. Typically, unbleached and bleached kraft pulp contains 3–8% and 0–1% lignin by mass, respectively, while TMP fibers contain 25–31% lignin [18].

3.2. Matrix composition

The composition of the C–S–H in the matrix was determined to investigate any changes in the chemical composition during wet/dry cycling. From BSE EDS, the Si/Ca in C–S–H was determined to be 0.520±0.031 both prior to and after wet/dry cycling. The determined ratio falls within the range of previously reported data [19].

In addition, C–S–H was assumed to have substituted some Al^{+3} for Si^{+4} and adsorbed some SO_4^{-2} [20]. Using the linear relationship between Si/Ca and Al/Ca in C–S–H developed by Richardson and Groves [21], a theoretical Al/Ca trace composition was estimated to be 0.02–0.05 based on the Si/Ca found in this research. In addition, experimental EDS analyses by Bonen and Diamond [22] showed that Al/Ca and S/Ca to be in the range from 0.034–0.066 and 0.037–0.060, respectively, in C–S–H with Si/Ca approximately 0.43–0.48.

In this research, prior to cycling, Al/Ca and S/Ca were determined to be 0.079±0.017 and 0.039±0.012, respectively. After 25 wet/dry cycles, these ratios were 0.069±0.015 and 0.031±0.010, respectively. These trace compositions are similar to those discussed previously. It is expected that Al/Ca would not vary during wet/dry cycling as aluminum is firmly bound within the C–S–H. However, since the sulfates are more loosely bound, these ions are more likely to desorb/adsorb within the C–S–H. However, desorption of sulfates from the C–S–H is not observed over the range of wet/dry cycles investigated in this research.

3.3. Composite microstructure prior to wet/dry cycling

EDS spot analyses for composite samples not exposed to wet/dry cycling can be seen in Figs. 4 and 5. Fig. 4 indicates that the dominant phases present on all fiber surfaces are typical of portland cement matrices: CH, C–S–H, and AFm/AFt phases.

The unbleached kraft pulp fibers appear to contain higher levels of the AFm/AFt phase than the other two fiber types. As for Fig. 5, it appears that the unbleached kraft fibers contain small amounts of ettringite (an AFt phase) on their fiber surface. The bleached fibers appear to contain both monosulfate (an AFm phase) and ettringite phases. The TMP fibers contain the lowest amount of monosulfate/ettringite and appear to primarily

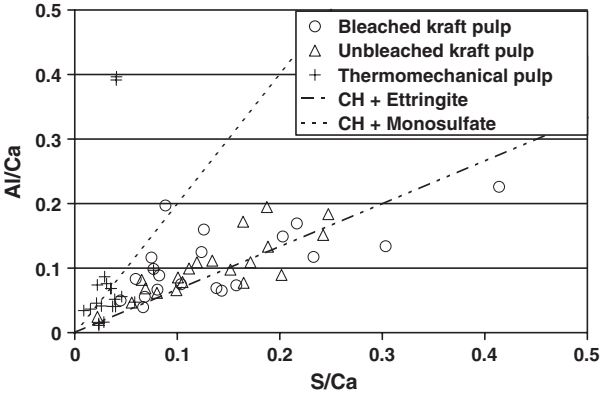

Fig. 9. Average Al/Ca versus S/Ca molar ratios after 2 cycles.

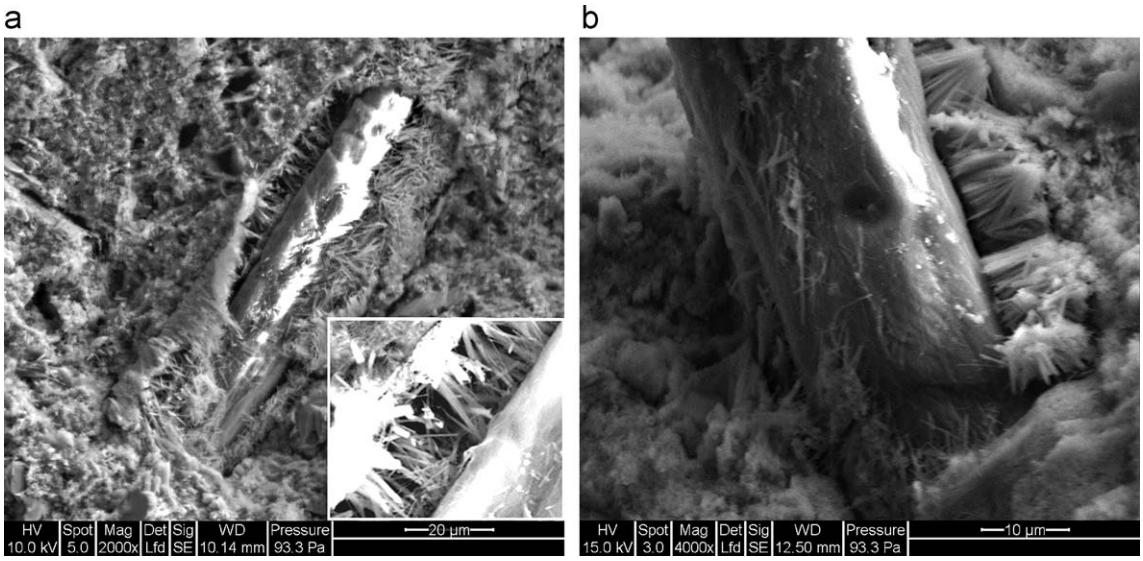

Fig. 10. ESEM micrographs after 2 wet/dry cycles. (a) Bleached kraft fiber composite showing needle-like ettringite formation between S1 and S2 fiber layers with closeup of ettringite crystals. (b) Bleached kraft fiber composite illustrating dense needle-like ettringite reprecipitation which restricts fiber swelling.

contain CH and C–S–H on the fiber surface. During fiber pull-out, prior to initial drying, the observed hydration products are assumed to be indicative of the surrounding matrix composition in the interfacial transition zone (ITZ).

3.4. Initial fiber–cement debonding

It is believed that fiber dimensional changes during wet/dry cycling, as discussed in Section 3.1, leads to fiber–cement debonding upon the initial drying cycle. ESEM observations also indicate that fiber interlayer debonding (e.g., debonding between the S1 and S2 layers) is also possible.

It is proposed that the debonding mode – whether initial debonding occurs at the fiber–cement interface or within the fiber cell wall – is most likely related to the degree of the fiber–cement bonding. That is, if the particular fiber–cement bond is stronger than the fiber interlayer bonding, interlayer debonding would be expected, and vice versa. Due to a physically rougher surface as a result of the removal of lignin during pulping and bleaching, bleached kraft fibers are expected to exhibit increased fiber–cement bonding and an increased tendency for fiber interlayer debonding, as compared to unbleached kraft fibers. Prior to cycling, fiber pull-out lengths for bleached kraft fibers have been shown to be shorter than that of unbleached kraft fibers [7]. Thus, the presence of lignin in unbleached kraft fibers does decrease fiber–cement bond strength and as a consequence, the tendency for fiber interlayer debonding is decreased as well.

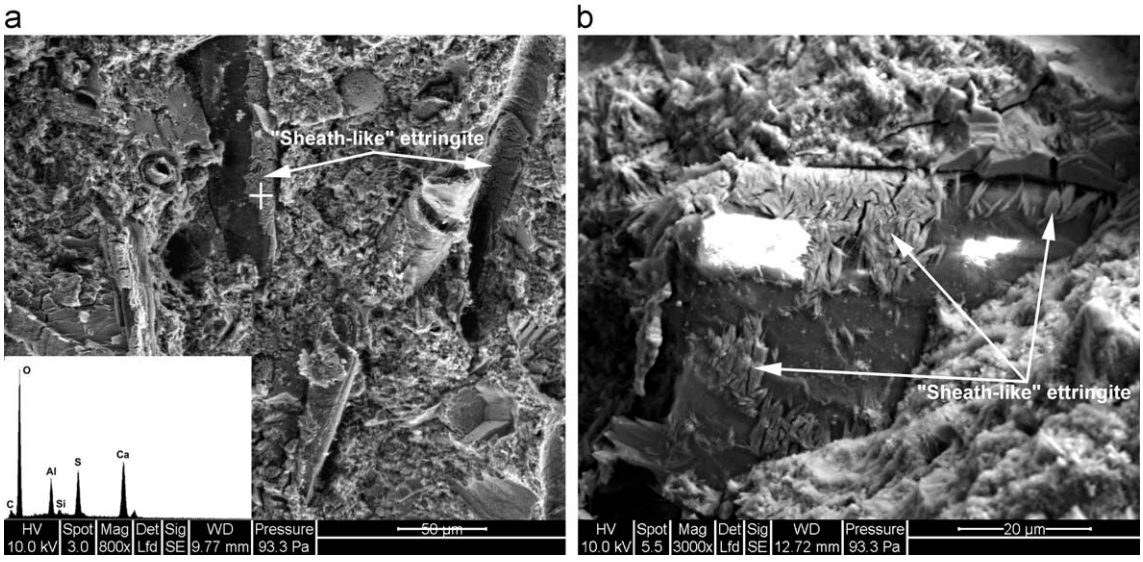

Fig. 11. ESEM micrographs after 2 wet/dry cycles. (a) Unbleached kraft fiber composite showed sheath-like ettringite formation and the corresponding EDS spectra confirming ettringite. (b) Closeup view of sheath-like ettringite formation around an unbleached kraft pulp fiber which exhibits fiber–cement debonding.

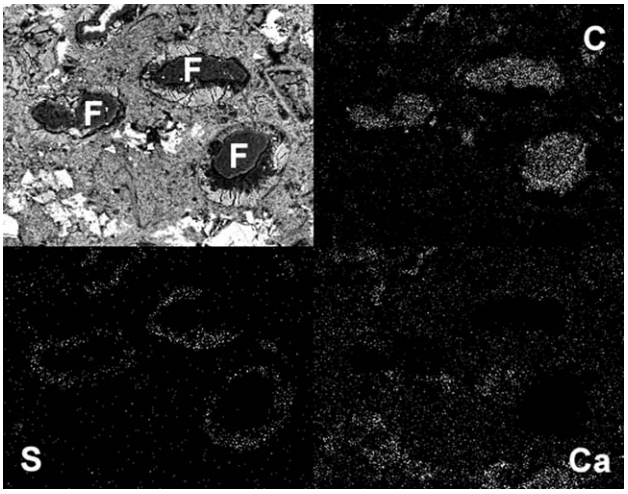

Fig. 12. ESEM BSE chemical mapping of polished kraft pulp fiber composite after 2 wet/dry cycles (upper right: carbon (C), lower left: sulfur (S), lower right: calcium (Ca)). Note: "F" indicates fiber.

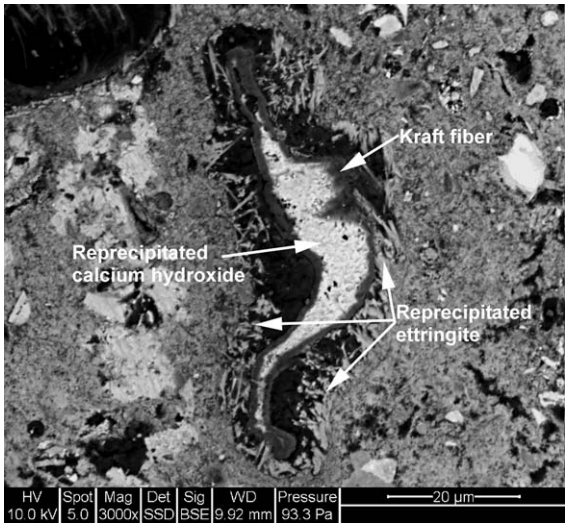

Fig. 14. ESEM BSE micrographs of kraft pulp fiber composites illustrating absence of microcracking around fibers due to ettringite reprecipitation.

EDS measurements obtained on samples subjected to 1 wet/dry cycle are shown in Figs. 6 and 7. For the kraft fibers, there are significant reductions in the amount of monosulfate, ettringite, and C–S–H present on the fiber surface, compared to Figs. 4 and 5, prior to cycling. Thus, it appears that CH is the dominant hydration product on the kraft fiber surface, though to a lesser extent for the unbleached kraft fibers. It should also be noted that increases in the Na/Ca and K/Ca molar ratios occurred after 1 wet/dry cycle for the unbleached kraft fibers only. This indicates that Na and K-rich products as well as CH have leached from the matrix and precipitated from the pore solution onto the unbleached kraft fiber surface. However, for the TMP fibers, there does not appear to be any observable changes in the relative abundances of alkali-rich products, C–S–H, and CH on the fiber surface.

Based on these observations, the TMP fibers exhibit negligible fiber–cement or fiber interlayer debonding upon drying. On the other hand, due to the removal of lignin, the bleached kraft fibers show considerable signs of fiber interlayer debonding. As the unbleached kraft fibers contain small amounts of lignin, they tend to show more fiber–cement debonding as evidenced by more C–S–H and precipitated alkali-rich products on their fiber surface, compared to the bleached kraft fibers. Regardless of the debonding mechanism – either fiber interlayer or fiber–cement – a void space is created due to this debonding. The void space created during this first step of the degradation model allows for the reprecipitation of ettringite upon subsequent wetting and drying as described in the following section.

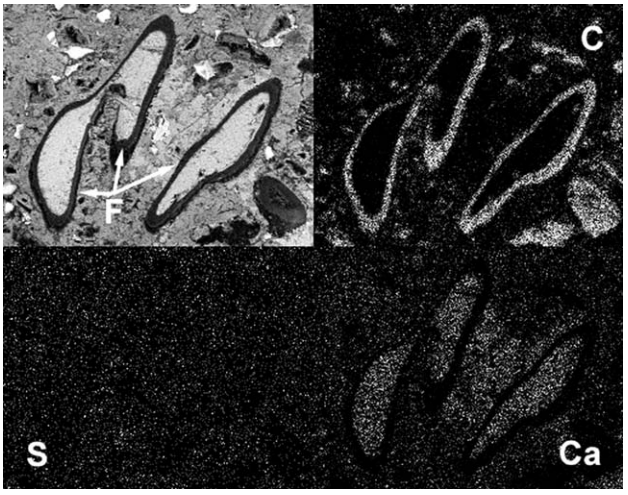

Fig. 13. ESEM BSE chemical mapping of polished TMP fiber composite after 25 wet/dry cycles (upper right: carbon (C), lower left: sulfur (S), lower right: calcium (Ca)). Note: "F" indicates fiber.

3.5. Reprecipitation of secondary ettringite

After fiber–cement or fiber interlayer debonding, the new void space acts as a reservoir for the pore solution and a repository of free ions during subsequent wetting. As seen in Figs. 8 and 9, significant changes in the bleached and unbleached kraft fiber surface compositions are apparent after 2 wet/dry cycles compared to that after 0 and 1 wet/dry cycle. As seen in these figures, there are noticeable increases in Al/Ca

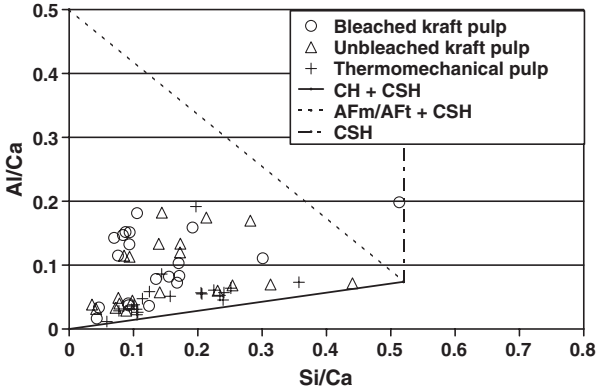

Fig. 15. Average Al/Ca versus Si/Ca molar ratios after 5 cycles.

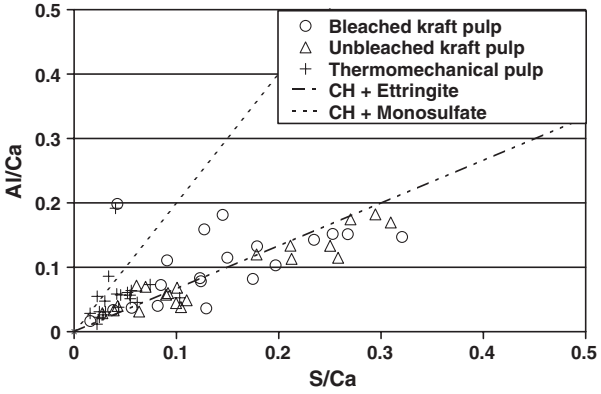

Fig. 16. Average Al/Ca versus S/Ca molar ratios after 5 cycles.

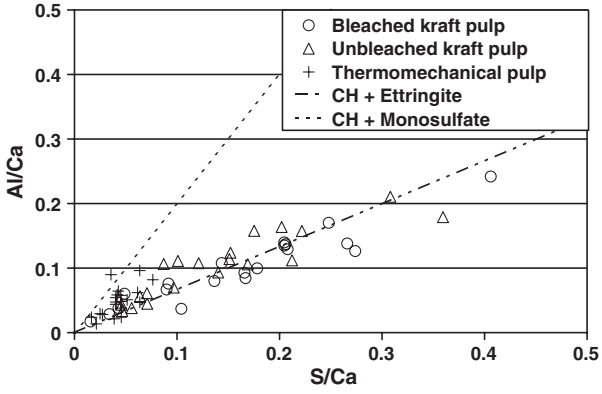

Fig. 18. Average Al/Ca versus S/Ca molar ratios after 10 cycles.

and S/Ca and decreases in Si/Ca for both kraft fiber types, suggesting the precipitation of sulfoaluminate products.

Fig. 9 definitively indicates the presence of ettringite around both kraft fiber types. Ettringite appears to be reprecipitating in the void space created by fiber–cement or fiber interlayer debonding. It is proposed that the formation of this secondary ettringite minimizes further debonding, as indicated by a relative stabilization in the values for first crack strength beyond 2 cycles and peak strength beyond 5 cycles [7,8].

In addition, there does not appear to be any observable change in the chemical composition at the TMP fiber surface, indicating that ettringite reprecipitation is prevented. Fiber–cement or fiber interlayer debonding of the TMP fibers is likely minimized due to the superior dimensional stability of these fiber compared to the kraft fibers, as described in Section 3.1. Thus, there is no available space for ettringite formation.

Batic et al. [23] have shown that the reprecipitation of ettringite in microcracks and voids of cement paste can occur under normal (i.e., non-elevated temperatures) curing conditions. As discussed in Section 3.2, the C–S–H does not appear to be the source for Ca^{+2}, $Al(OH)_4^-$, and/or SO_4^{-2} participating in the formation of ettringite. In addition, though the kraft pulping process involves soaking the fibers in a sulfate solution, it was shown in Section 3.1 that the kraft fibers do not contain excess sulfates that could be contributing to ettringite formation. Thus, the additional sulfate required for ettringite formation may be provided by existing monosulfate and/or ions in the pore solution. Monosulfate is most likely also the source of $Al(OH)_4^-$, as these ions are not generally abundant in the pore solution during hydration [24,25].

Upon rewetting after the initial drying cycle, Ca^{+2} (primarily from CH and monosulfate) and SO_4^{-2} may react with $Al(OH)_4^-$ provided by monosulfate to form ettringite. Additionally, it is thought that accelerated leaching of Na^+ and K^+ (Ca^{+2} is maintained due to limewater saturation) due to cycling and the subsequent lowering of pore solution pH occurs within the first 2 wet/dry cycles. Leaching was observed through a reduction in K/Ca and Na/Ca by 2 cycles. These aspects favor ettringite formation and the destabilization of monosulfate [25].

Fig. 10 illustrates the formation of needle-like crystals, believed to be ettringite based on EDS data, near kraft fibers after 2 wet/dry cycles. Based on visual observation, the typical needle-like ettringite crystals only appear to form in cases of fiber interlayer debonding where the S1 fiber layer remained attached to the matrix. However, such needle-like crystals are not observed on all fiber surfaces (Fig. 11), despite EDS spot analyses indicating the presence of ettringite.

Products matching EDS spectra for ettringite are also observed around the circumference of some kraft fibers, forming a sheath-like structure, similar to ASR gel [26], as seen in Fig. 11. The "sheath-like" ettringite crystallographic *c*-axis is parallel to the outer fiber surface, as previously observed in heat-treated specimens by Siedel et al. [27].

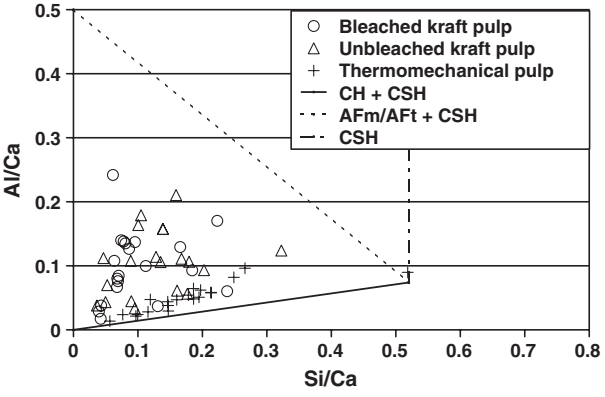

Fig. 17. Average Al/Ca versus Si/Ca molar ratios after 10 cycles.

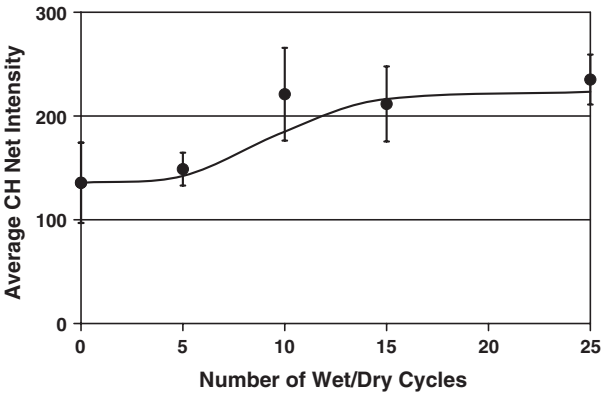

Fig. 19. Average ESEM EDS CH net intensity (abundance) in bleached and unbleached kraft fiber cell walls.

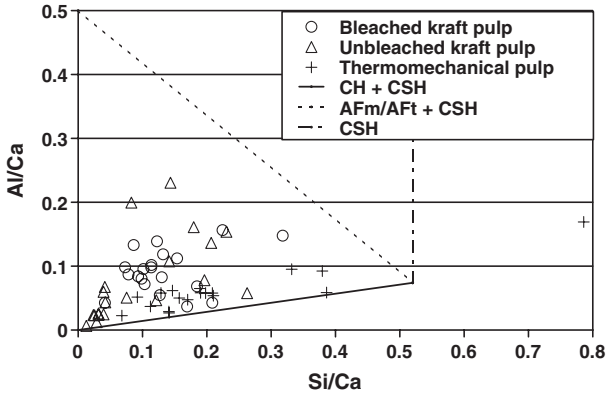

Fig. 20. Average Al/Ca versus Si/Ca molar ratios after 15 cycles.

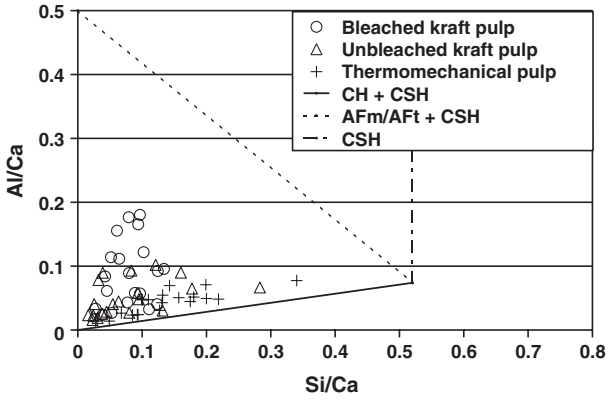

Fig. 22. Average Al/Ca versus Si/Ca molar ratios after 25 cycles.

It is proposed that the form of ettringite reprecipitation – needle-like or sheath-like – is likely dependent upon the fiber–cement debonding mechanism. Sheath-like ettringite appears to form only in the case of fiber–cement debonding (primarily unbleached kraft fibers). It was previously mentioned that needle-like crystals formed when fiber interlayer debonding was observed (primarily bleached kraft fibers). Thus, the form of ettringite is likely also to be inherently related to the available space for reprecipitation. Fiber interlayer debonding creates a space of 10–15 μm, while fiber–cement debonding appears to create a void space width of only a few microns. Therefore, a more constrained void space appears to favor sheath-like ettringite.

Ettringite formation was also verified via chemical elemental mapping of polished samples. Fig. 12 shows distinct rings of ettringite around several kraft pulp fibers after 2 wet/dry cycles. As for the TMP fibers, ettringite formation was not observed, even after 25 cycles as seen in Fig. 13.

In addition, no radial microcracking was observed around the kraft pulp fibers after 25 wet/dry cycles, as indicated in Fig. 14. Thus, ettringite reprecipitation does not appear to be exerting tensile stresses against the cement matrix which exceed the tensile strength of this region. Since the pulp fibers are more compliant, however, the ettringite formation most likely exerts some pressure on the fiber, eventually restricting fiber swelling.

With subsequent wetting and drying there are no apparent changes in fiber surface composition, as indicated by Figs. 15 and 16 (5 cycles) and Figs. 17 and 18 (10 cycles), compared to that after 2 cycles.

3.6. Fiber mineralization

After ettringite reprecipitation around the fibers, fiber swelling upon wetting is expected to be limited or prevented. Fiber shrinkage, upon subsequent drying, is also significantly minimized or prevented. Thus, the capillary forces thought to be responsible for initially expelling the pore solution from the fiber lumen are minimized. Therefore, during drying, the pore solution may diffuse from the lumen through the cell wall, resulting in a deposition of hydration products, likely CH.

It was previously proposed that complete mineralization of bleached and unbleached kraft fibers may not occur until after 10 wet/dry cycles as indicated by slight increases in flexural strength [7]. EDS measurements of relative CH content within the kraft fiber cell walls as a function of the number of wet/dry cycles are shown in Fig. 19. A sharp increase in the CH content occurs between 5 and 10 wet/dry cycles, indicating kraft fiber mineralization due to CH reprecipitation within their cell wall. In addition, after 15 and 25 wet/dry cycles (Figs. 20–23), increasing amounts of CH are present on the kraft fiber surfaces,

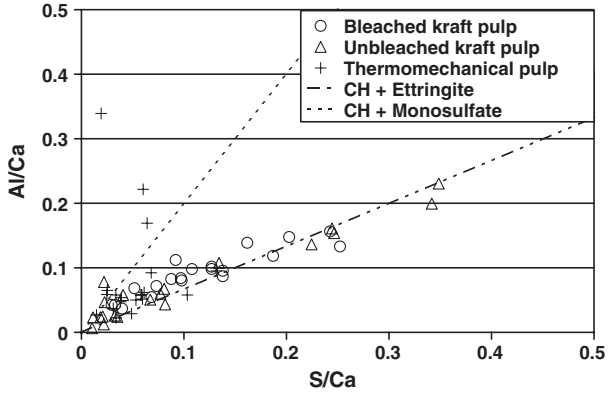

Fig. 21. Average Al/Ca versus S/Ca molar ratios after 15 cycles.

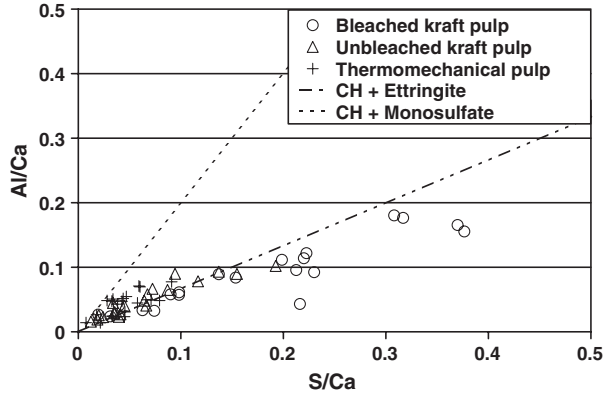

Fig. 23. Average Al/Ca versus S/Ca molar ratios after 25 cycles.

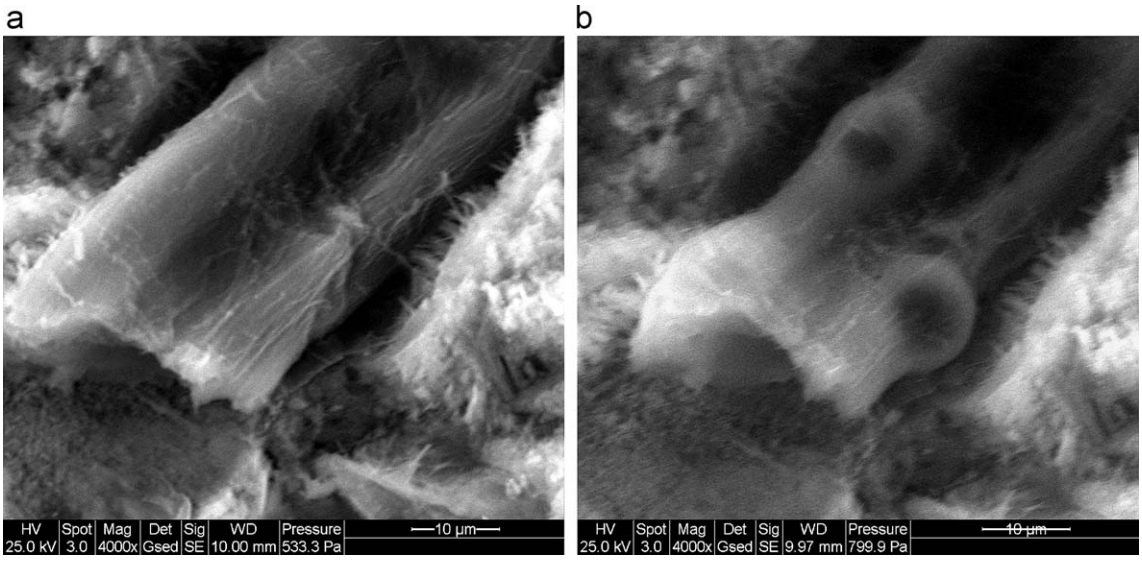

Fig. 24. ESEM micrograph of kraft pulp fiber after 25 wet/dry cycles. (a) Prior to saturation (10% RH). (b) After 1 h at 98% RH.

evidenced by a progressive decrease of the observed molar ratios from 10 to 25 cycles.

Additional ESEM observations were made during in situ wetting and drying of composite fracture surfaces to observe the swelling behavior and extent of fiber mineralization of kraft pulp fibers after 25 wet/dry cycles. It can be seen in Fig. 24 that localized kraft fiber swelling is apparent, but overall fiber swelling (as seen in Fig. 3) is restricted. Complete fiber mineralization (i.e., no fiber swelling) by the reprecipitation of CH in the fiber cell wall is also apparent in most kraft fibers as seen in Fig. 25. Fig. 26 shows a completely mineralized kraft fiber and the corresponding EDS spectra of the fiber surface. However, levels of organic materials remain relatively high, indicating that replacement of organic with inorganic components does not appear to be occurring. Instead, it is believed that CH reprecipitates within the fiber wall by filling the space between the cellulose microfibrils. This space would have been previously occupied by lignin prior to kraft pulping.

In TMP fibers, the space within the fiber cell wall is occupied by lignin as it is not removed during thermomechanical pulping. TMP fibers, after 25 cycles (Fig. 27), exhibit minimal levels of calcium on the fiber surface and/or in the fiber cell wall as evidenced by the EDS spectrum. However, TMP fibers do show evidence of CH formation within the fiber lumen. This is particularly evident in Fig. 13, where calcium is the predominant element observed within the fiber lumen. Thus, it is thought that lignin within the TMP fiber cell wall acts as a barrier to pore solution ingress/egress and by its very presence prevents reprecipitation of mineral phases within the fiber cell wall minimizing fiber mineralization.

It is proposed that calcium hydroxide may be accumulating in the TMP fiber lumen due to the superior dimensional

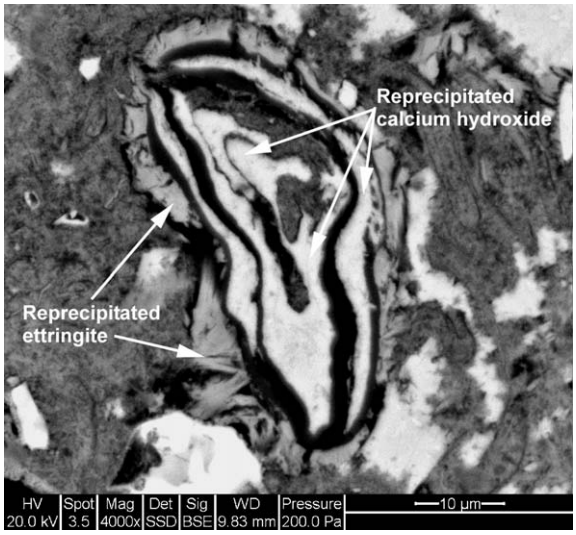

Fig. 25. ESEM BSE micrograph of a kraft fiber after 25 wet/dry cycles showing extent of calcium hydroxide reprecipitation.

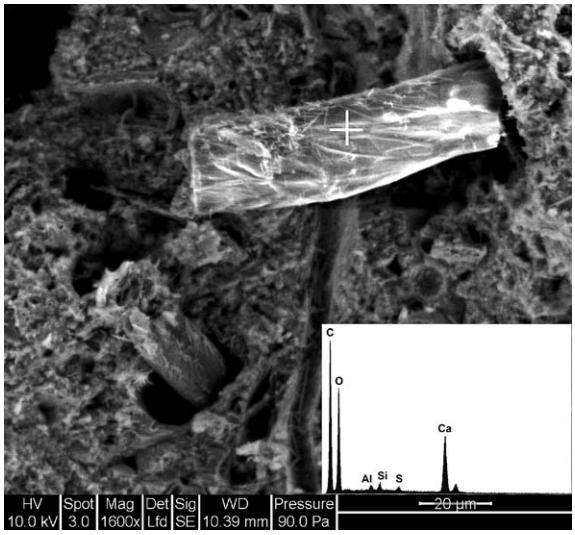

Fig. 26. ESEM micrograph of kraft fiber after 25 wet/dry cycles illustrating complete fiber mineralization and corresponding EDS spectra of fiber surface.

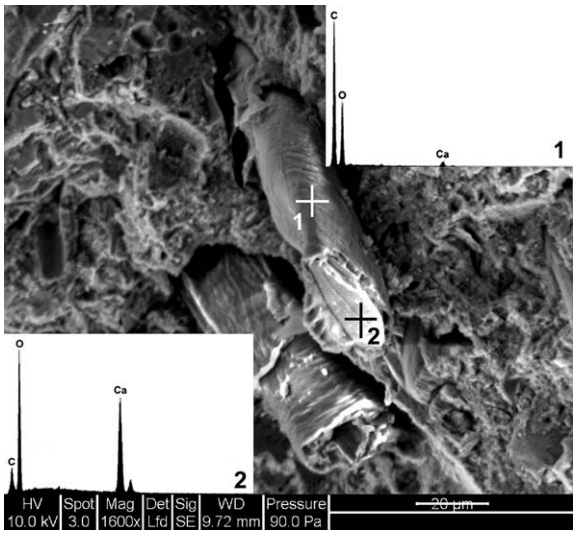

Fig. 27. ESEM micrograph of TMP fiber after 25 wet/dry cycles showing calcium hydroxide reprecipitation in fiber lumen only as evidenced by corresponding EDS spectra of fiber surface and mineral phases in fiber lumen.

stability of TMP fibers. Since TMP fibers exhibit negligible fiber shrinkage upon drying, the driving force for pore solution expulsion is minimized. This is similar to what has been proposed concerning ettringite reprecipitation around kraft fibers preventing subsequent fiber swelling/shrinkage [7]. However, in the case of kraft fibers during latter drying cycles (after ettringite formation), the pore solution may filter through the fiber cell wall, depositing CH. Pore solution movement through the TMP fiber cell wall is minimized, if not prevented, due to lignin, leading to the accumulation of CH within the fiber lumen.

4. Conclusions

Kraft pulp and TMP fiber–cement composites subjected to 0, 1, 2, 5, 10, 15, or 25 cycles were examined by ESEM for microstructural and microchemical changes in the fibers themselves (considering the fiber surface, cell wall, and lumen) and in the surrounding matrix, including the interfacial transition zone. From the ESEM observations, the following conclusions may be made:

- Kraft pulp fibers exhibit poor dimensional stability, as compared to TMP fibers, prior to incorporation within a cement matrix.
- Kraft fiber–cement or fiber interlayer debonding occurs during the initial drying cycle. It was observed that bleached kraft fibers tended to exhibit fiber interlayer bonding while unbleached kraft fibers typically exhibited fiber–cement debonding. No debonding or changes in the chemical composition of the TMP fibers were observed after 1 wet/dry cycle.
- Ettringite reprecipitation was found to occur around the kraft pulp fibers only. As visually and chemically confirmed, ettringite formation occurred after 2 wet/dry cycles. The observed ettringite morphology, needle-like or sheath-like, appears to be dependent upon the debonding mechanism (i.e., debonding at the fiber–cement interface or with the fiber cell wall) which influences the relative void widths. This reprecipitation around kraft fibers is proposed to have prevented subsequent fiber swelling/shrinkage.
- Kraft pulp fiber embrittlement results from the reprecipitation of CH within the fiber cell wall and lumen. ESEM EDS observations confirmed relatively constant fiber organic content but significantly increased inorganic content within the bleached and unbleached kraft fiber cell walls. TMP fibers were observed to minimize fiber mineralization due to the presence of lignin in the spaces within the fiber cell wall. Calcium hydroxide was observed to only precipitate within the fiber lumen of TMP fibers.
- This research validates the proposed three-step progressive degradation model for bleached and unbleached kraft pulp (low-lignin content) fiber–cement composites subjected to wet/dry cycling. It has been shown that ettringite reprecipitation is largely dependent upon the occurrence of fiber–matrix debonding. Similarly, calcium hydroxide reprecipitation within the pulp fiber cell wall is dependent upon the first two mechanisms. Therefore, changes to the initial step(s) may influence the overall degradation behavior. Thus, this model can also be used to elucidate the mechanisms of improved TMP composite durability by comparison to kraft fiber composite performance.

Acknowledgements

The authors would like to acknowledge the National Science Foundation (CMS-0556015, CMS-0122068, and DMR-0115961), the Institute of Paper Science and Technology (IPST)/Georgia Tech seed grant program, and IPST PATHWAYS program for their financial support. Dr. Hiroki Nanko is thanked for obtaining the fibers used in this study and for providing invaluable technical assistance regarding pulp fiber chemistry and morphology. Any opinions, findings, and conclusions or recommendations expressed in this material are those of the authors and do not necessarily reflect the views of the sponsors.

References

[1] S. Marikunte, P. Soroushian, Statistical evaluation of long-term durability characteristics of cellulose fiber reinforced cement composites, ACI Mater. J. 91 (6) (1994) 607–616.
[2] H. Gram, Methods for reducing the tendency towards embrittlement in sisal fibre concrete, Nordic Concr. Res. 2 (1983) 62–71.
[3] P. Soroushian, S. Marikunte, J. Won, Wood fiber reinforced cement composites under wetting-drying and freezing-thawing cycles, J. Mater. Civ. Eng. 6 (4) (1994) 595–611.
[4] R.D. Tolêdo Filho, G.L. England, K. Ghavami, K. Scrivener, Development of vegetable fibre-mortar composites of improved durability, Cem. Concr. Compos. 25 (2003) 185–196.
[5] N.H. El-Ashkar, B.J. Mohr, H. Nanko, K.E. Kurtis, Durability of pulp fiber–cement composites to wet/dry cycling, in: M. Anson, J.M. Ko, E.S.S. Lam (Eds.), Proceedings of the International Conference on Advances in Building Technology, Elsevier, Oxford, 2002, pp. 233–237.
[6] S.A.S. Akers, J.B. Studinka, Ageing behavior of cellulose fibre cement composites in natural weathering and accelerated tests, Int. J. Cem. Compos. Lightweight Concr. 11 (2) (1989) 93–97.

[7] B.J. Mohr, H. Nanko, K.E. Kurtis, Durability of kraft pulp fiber–cement composites to wet/dry cycling, Cem. Concr. Compos. 27 (5) (2005) 435–448.
[8] B.J. Mohr, H. Nanko, K.E. Kurtis, Durability of thermomechanical fiber–cement composites to wet/dry cycling, Cem. Concr. Res. 35 (8) (2005) 1646–1649.
[9] ACI544.1R, State-of-the-art Report on Fiber Reinforced Concrete, American Concrete Institute, Detroit, Michigan, USA, 1996.
[10] M.D. Campbell, R.S.P. Coutts, Wood fibre-reinforced cement composites, J. Mater. Sci. 15 (8) (1980) 1962–1970.
[11] A. Bentur, S.A.S. Akers, The microstructure and ageing of cellulose fibre reinforced cement composites cured in a normal environment, Int. J. Cem. Compos. Lightweight Concr. 11 (2) (1989) 99–109.
[12] R.D. Tolêdo Filho, K. Scrivener, G.L. England, K. Ghavami, Durability of alkali-sensitive sisal and coconut fibres in cement mortar composites, Cem. Concr. Compos. 22 (6) (2000) 127–143.
[13] H. Savastano, V. Agopyan, Transition zone studies of vegetable fibre-cement paste composites, Cem. Concr. Compos. 21 (1999) 49–57.
[14] J.M. Richardson, J.J. Biernacki, P.E. Stutzmann, D.P. Bentz, Stoichiometry of slag hydration with calcium hydroxide, J. Am. Ceram. Soc. 85 (4) (2002) 947–953.
[15] K.E. Kurtis, H. Nanko, N.H. El-Ashkar, US Patent 20020160174, 6 November 2001.
[16] N.H. El-Ashkar, H. Nanko, K.E. Kurtis, Investigation of flexural properties of wood pulp microfiber cement-based composites, in: A.S. El-Dieb, S.L. Lissel, M.M. Reda Taha (Eds.), Proceedings of the International Conference on Performance of Construction Materials in the New Millennium, Cairo, Egypt, 2003, pp. 1055–1064.
[17] H. Nanko, S. Asano, J. Ohsawa, Shrinkage behavior of pulp fibers during drying, Proceedings of TAPPI International Paper Physics Conference, Kona, HI, 1991, pp. 365–374.
[18] P. Stenius, Forests Products Chemistry, TAPPI, Atlanta, 2000.
[19] H.F.W. Taylor, Cement Chemistry, Thomas Telford, London, 1997.
[20] I.G. Richardson, The nature of C–S–H in hardened cement pastes, Cem. Concr. Res. 29 (8) (1999) 1131–1147.
[21] I.G. Richardson, G.W. Groves, Incorporation of minor and trace elements into calcium silicate hydrate (C–S–H) gel in hardened cement pastes, Cem. Concr. Res. 23 (1) (1999) 131–138.
[22] D. Bonen, S. Diamond, Interpretation of compositional patterns found by quantitative energy dispersive X-ray analysis for cement paste constituents, J. Am. Ceram. Soc. 77 (7) (1994) 1875–1882.
[23] O.R. Batic, C.A. Milanesi, P.J. Maiza, S.A. Marfil, Secondary ettringite formation in concrete subjected to different curing conditions, Cem. Concr. Res. 30 (2000) 1407–1412.
[24] T. Ramlochan, M.D.A. Thomas, R.D. Hooton, The effect of pozzolans and slag on the expansion of mortars cured at elevated temperature, Part II: microstructural and microchemical investigations, Cem. Concr. Res. 34 (2004) 1341–1356.
[25] H.F.W. Taylor, C. Famy, K.L. Scrivener, Delayed ettringite formation, Cem. Concr. Res. 31 (2001) 683–693.
[26] S.L. Marusin, A simple treatment to distinguish alkali-silica gel from delayed ettringite formation in concrete, Mag. Concr. Res. 46 (168) (1994) 163–167.
[27] H. Siedel, S. Hempel, R. Hempel, Secondary ettringite formation in heat treated portland cement concrete: influence of different w/c ratios and heat treatment temperatures, Cem. Concr. Res. 23 (1993) 453–461.